

# SCIENTIFIC REPORTS



OPEN

## Transport and retention of engineered $\text{Al}_2\text{O}_3$ , $\text{TiO}_2$ , and $\text{SiO}_2$ nanoparticles through various sedimentary rocks

Ali Esfandyari Bayat<sup>1</sup>, Radzuan Junin<sup>1</sup>, Shahaboddin Shamshirband<sup>2</sup> & Wen Tong Chong<sup>3</sup>

Received: 21 April 2015

Accepted: 21 August 2015

Published: 16 September 2015

Engineered aluminum oxide ( $\text{Al}_2\text{O}_3$ ), titanium dioxide ( $\text{TiO}_2$ ), and silicon dioxide ( $\text{SiO}_2$ ) nanoparticles (NPs) are utilized in a broad range of applications; causing noticeable quantities of these materials to be released into the environment. Issues of how and where these particles are distributed into the subsurface aquatic environment remain as major challenges for those in environmental engineering. In this study, transport and retention of  $\text{Al}_2\text{O}_3$ ,  $\text{TiO}_2$ , and  $\text{SiO}_2$  NPs through various saturated porous media were investigated. Vertical columns were packed with quartz-sand, limestone, and dolomite grains. The NPs were introduced as a pulse suspended in aqueous solutions and breakthrough curves in the column outlet were generated using an ultraviolet-visible spectrophotometer. It was found that  $\text{Al}_2\text{O}_3$  and  $\text{TiO}_2$  NPs are easily transported through limestone and dolomite porous media whereas NPs recoveries were achieved two times higher than those found in the quartz-sand. The highest and lowest  $\text{SiO}_2$ -NPs recoveries were also achieved from the quartz-sand and limestone columns, respectively. The experimental results closely replicated the general trends predicted by the filtration and DLVO calculations. Overall, NPs mobility through a porous medium was found to be strongly dependent on NP surface charge, NP suspension stability against deposition, and porous medium surface charge and roughness.

Nowadays, many industries such as food processing, cosmetics, pigments, paints, and electronics are producing and utilizing engineered metal oxide nanoparticles (NPs) such as aluminum oxide ( $\text{Al}_2\text{O}_3$ ), titanium dioxide ( $\text{TiO}_2$ ), and silicon dioxide ( $\text{SiO}_2$ )<sup>1,2</sup>. This has led to noticeable quantities of these NPs to be released into the environment daily. Since the toxicity of these metal oxide NPs is greater than the toxicity of bulk formulations with the same chemistry<sup>3</sup>, their release and accumulation into the environment has caused adverse influences on aquatic organisms such as microbes, algae, fish, and invertebrates<sup>4-6</sup>. Metal oxide NPs especially  $\text{Al}_2\text{O}_3$  and  $\text{TiO}_2$  have been also classified as carcinogenic to humans by the international agency for research on cancer (IARC)<sup>4,7</sup>. A portion of the released NPs can be transferred into the subsurface layers. Since NPs have tiny dimensions, they have the potential to be transported into subsurface alluvial zones<sup>8-9</sup>. Thus, there is a high risk that NPs can reach and contaminate drinking groundwater resources. As the physical and chemical properties of subsurface media are extremely complex, issues of how and where the NPs are distributed into the subsurface still remain major challenges for environmental engineering<sup>2,10</sup>.

<sup>1</sup>UTM-MPRC Institute for Oil and Gas, N29A, Lengkuu Suria, Universiti Teknologi Malaysia, 81310, UTM Skudai, Johor Bahru, Malaysia. <sup>2</sup>Department of Computer System and Information Technology, Faculty of Computer System and Information Technology, University of Malaya, 50603 Kuala Lumpur, Malaysia. <sup>3</sup>Department of Mechanical Engineering, Faculty of Engineering, University of Malaya, 50603 Kuala Lumpur, Malaysia. Correspondence and requests for materials should be addressed to R.J. (email: radzuan@petroleum.utm.my) or A.E.B. (email: ali.esfandyari.bayat@petroleum.utm.my)

Metal oxide NPs (i.e. Al<sub>2</sub>O<sub>3</sub>, TiO<sub>2</sub>, and SiO<sub>2</sub>) have also been recently introduced as agents for enhanced oil recovery (EOR) from hydrocarbon reservoirs<sup>11–13</sup>. The use of NPs for EOR purposes is a new application in petroleum engineering and needs to be tested and validated before the NPs are fully utilized. NPs usage for EOR is also facing the same question of how NPs are transported through the hydrocarbon reservoirs. NPs can precipitate in hydrocarbon reservoir pores and consequently clog them during transport<sup>14</sup>. Thereby, the permeability of reservoir is reduced which results in a decline of hydrocarbon reservoir productivity. Thus, prior to the use of NPs for EOR implementation, the effects of different parameters on the NPs transport of porous media should be investigated.

As discussed earlier, transport and retention of engineered metal oxide NPs in subsurface natural porous media are important issues for both environmental and petroleum engineering. To date, comprehensive studies on transport and retention of the engineered Al<sub>2</sub>O<sub>3</sub> and TiO<sub>2</sub> NPs under some environmentally relevant conditions have been carried out. For example, The effects of different physicochemical parameters such as size, concentration, and shape of NPs<sup>2,15–19</sup>, NP surface coating with surfactant, polymer and or NOM<sup>20–24</sup>, fluid velocity<sup>9,15,25</sup>, solution chemistry (i.e. ionic strength, pH, and ion type)<sup>21,26–30</sup>, and presence of clay particles<sup>31–33</sup> on the transport and retention of the Al<sub>2</sub>O<sub>3</sub> and TiO<sub>2</sub> NPs have been determined. However, there are some other parameters that still must to be evaluated. For example, porous media physics and chemistry are parameters which their effects on NPs transport have not yet been fully understood. The earth's crust is composed of different sedimentary rocks such as sandstones, conglomerates, carbonates, and so on<sup>34</sup>. According to the literature, quartz-sands and soils are two most common types of porous media utilized in previous studies on the NPs transport<sup>2,9,15,21,31,35–37</sup>. To the best of our knowledge, other porous media types such as carbonate porous media (i.e. limestones and dolomites) have not been fully studied for the NPs transport. Carbonates are a class of sedimentary rocks which form about 15% of the earth's sedimentary crust<sup>34</sup>. A considerable portion of underground water resources is located within the carbonate rocks<sup>29</sup>. In addition, approximately 40% of the discovered hydrocarbon resources in the world is in the carbonate rocks<sup>38,39</sup>. Thus, more studies are in demand to evaluate the NPs transport behavior through carbonate rocks. Consequently, the role of porous media physics and chemistry on NPs transport will be figured out.

This study was designed to investigate and compare the influences of three sedimentary rocks (i.e. limestone, dolomite, and quartz-sand) on transport and retention behavior of three metal oxide NPs, namely Al<sub>2</sub>O<sub>3</sub>, TiO<sub>2</sub>, and SiO<sub>2</sub>. To achieve this aim, laboratory scale column experiments were carried out to determine the amount of Al<sub>2</sub>O<sub>3</sub>, TiO<sub>2</sub>, and SiO<sub>2</sub> NPs retention in limestone, dolomite, and quartz sand porous media. Tests included ultraviolet-visible (UV-VIS) spectrophotometer, dynamic light scattering (DLS) and zeta potential ( $\zeta$ -potential) techniques which were performed to measure the NP concentration, size and surface charge, respectively. Furthermore, the classical Derjaguin–Landau–Verwey–Overbeek (DLVO) and filtration theories were applied to assess and explain the NPs deposition and maximum transport distance through porous media.

## Results and Discussion

**Nanoparticles Characterizations.** The average size of Al<sub>2</sub>O<sub>3</sub>, TiO<sub>2</sub>, and SiO<sub>2</sub> nanopowders was measured by two methods. Firstly, X-ray diffraction (XRD) analysis and Scherrer's formula<sup>40</sup> were used as follows:

$$d_{hkl} = \frac{0.9 \lambda}{B \cos \theta_B} \quad (1)$$

where  $d_{hkl}$  is the mean NP size (nm),  $B$  (radians) comprises the full width at half-maximum of the broadened diffraction line observed at the  $2\theta$  angular range,  $\lambda$  is the wavelength of Cu K $_{\alpha}$  radiation ( $\lambda = 0.1542$  nm) and  $\theta_B$  is the Bragg angle of diffraction.

The XRD analysis from aluminum oxide sample demonstrated that NP has alpha ( $\alpha$ ) crystalline structure and its composition is pure Al<sub>2</sub>O<sub>3</sub> (Fig. 1a). TiO<sub>2</sub> and SiO<sub>2</sub> NPs have partial amorphous (semi-crystalline) structures. The former has a composition of anatase while the latter has quartz composition as shown in Fig. 1b,c. Furthermore, from the equation, the sizes of Al<sub>2</sub>O<sub>3</sub>, TiO<sub>2</sub>, and SiO<sub>2</sub> NPs were calculated and found to be 26, 11.8, and 16.1 nm respectively. The sizes of Al<sub>2</sub>O<sub>3</sub>, TiO<sub>2</sub>, and SiO<sub>2</sub> nanopowders were also measured by TEM and image-processing software (ImageJ; National Institute of Mental Health). The geometric means of Al<sub>2</sub>O<sub>3</sub>, TiO<sub>2</sub>, and SiO<sub>2</sub> NPs diameter measured were 25 (12–138), 6 (3–65), and 13 (7–81) nm respectively. Therefore, there is a 35% to 40% difference in the size of the NPs depending on whether it was measured by XRD and TEM or reported by the manufacturer. Furthermore, according to TEM images, the morphology of NPs appeared to be spherical (Fig. 1).

The  $\zeta$ -potential values of Al<sub>2</sub>O<sub>3</sub>, TiO<sub>2</sub> and SiO<sub>2</sub> NPs in DIW were also measured to be  $+19.1 \pm 0.3$ ,  $+9.1 \pm 0.3$ , and  $-28.1 \pm 0.3$  mV respectively. Besides that, the sizes of Al<sub>2</sub>O<sub>3</sub>, TiO<sub>2</sub>, and SiO<sub>2</sub> NP aggregates in DIW were measured to be 255 (75–510), 220 (65–440), and 280 (80–620) nm respectively using the DLS probe. The DLS analyses depict that the hydraulic size of Al<sub>2</sub>O<sub>3</sub>, TiO<sub>2</sub>, and SiO<sub>2</sub> NPs in DIW is much greater than the size of NPs in the powder form. Thus, it can be concluded that these NPs aggregated in DIW.

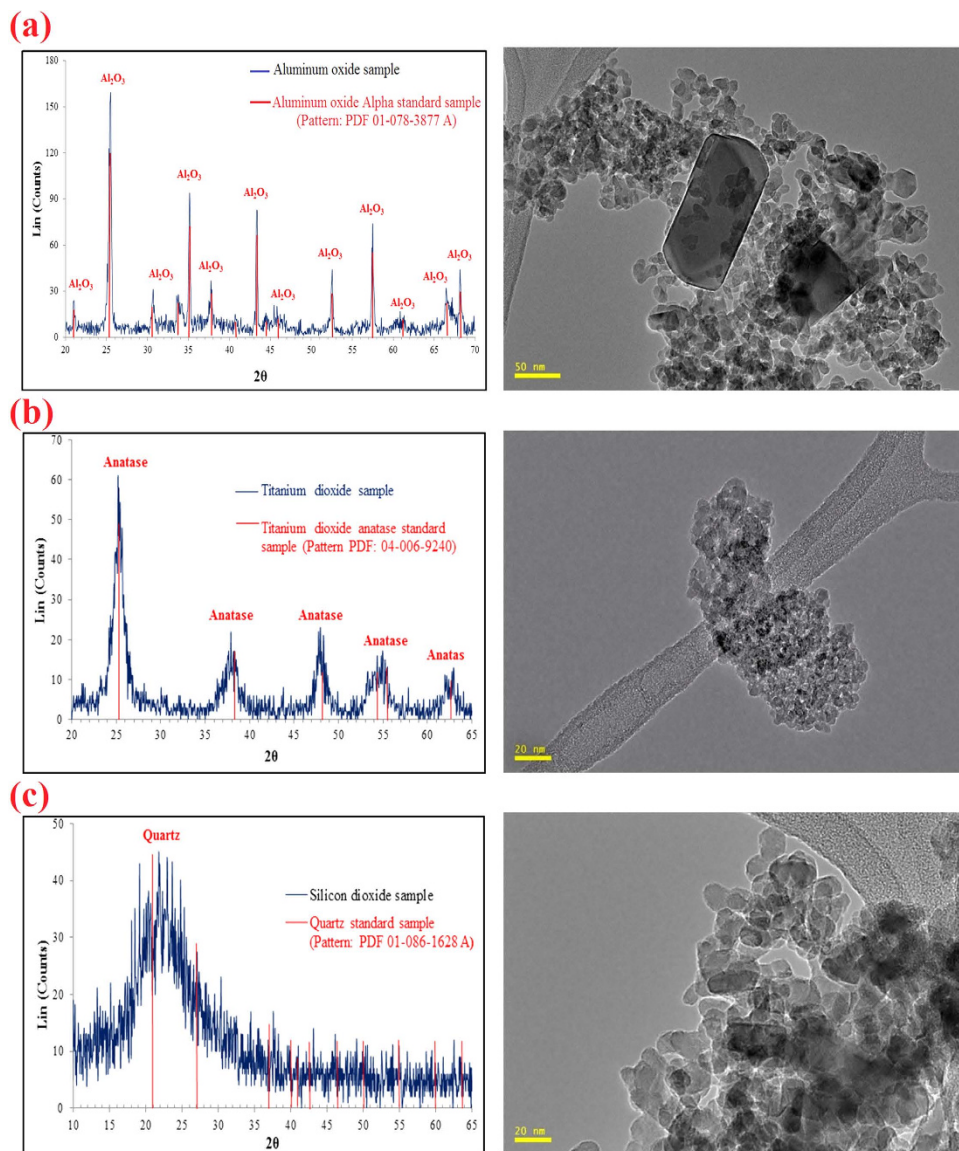


**Figure 1.** XRD (left) and TEM (right) analyses from the nanopowders (a)  $\text{Al}_2\text{O}_3$ -NPs, (b)  $\text{TiO}_2$ -NPs, (c)  $\text{SiO}_2$ -NPs.

**Sedimentation tests results.** The sedimentation tests results revealed that the stability of  $\text{SiO}_2$ -NPs against deposition in static condition was higher than  $\text{Al}_2\text{O}_3$  and  $\text{TiO}_2$  NPs during 180 min (Fig. 2a). The interaction between NPs is one of the factors which determines the NPs stability in a dispersion medium<sup>29</sup>. For this finding, DLVO theory was applied to qualitatively explain this interaction<sup>41</sup>. The interaction between two particles can either be attraction or repulsion. The electrostatic double layer (EDL) is a force which drives particles apart while the van der Waals (VDW) force drives particles toward each other. The summation of these forces clarifies whether the net interaction between two particles is attractive or repulsive<sup>42</sup>. High positive values of the total interaction energy imply that the EDL force is greater in magnitude and the dominant force<sup>29</sup>. The total interaction energy for NP-NP as a function of distance for the  $\text{Al}_2\text{O}_3$ ,  $\text{TiO}_2$ , and  $\text{SiO}_2$  NPs was calculated and drawn. As shown in Fig. 2b, the EDL is the dominant force among all NPs. However, the interaction energy height for  $\text{SiO}_2$ -NPs is higher than  $\text{Al}_2\text{O}_3$  and  $\text{TiO}_2$  NPs which reveals a higher repulsion force among  $\text{SiO}_2$ -NPs. Consequently,  $\text{SiO}_2$ -NP suspension is more stable than  $\text{Al}_2\text{O}_3$  and  $\text{TiO}_2$  NPs suspensions. Therefore, DLVO theory supports these experimental results.

It should be pointed that for applying filtration theory, the condition should be steady state during the transport tests<sup>21</sup>. According to 1 ml/min injection rate and number of injected PVs (2PVs) during the experiments, 18 min is required to deliver the NPs suspensions into the porous media. Based on the optical absorbency results (Fig. 2a), for the first 20 min of the experiments, NPs sedimentation values

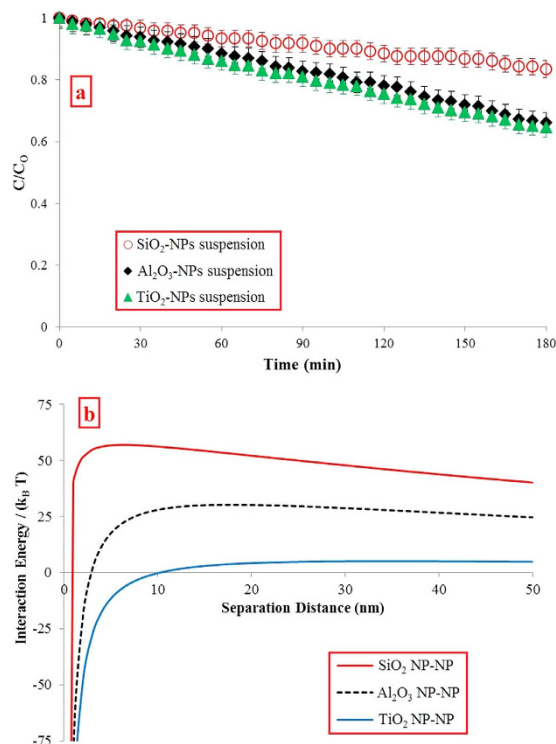


**Figure 2.** (a) Sedimentation tests results, (b) NP-NP interaction energy profiles generated by DLVO theory.

are less than 5 wt% of the initial value (0.005 wt%) that is negligible. Thus, it is justifiable to apply the transport theory for steady-state systems.

**Nanoparticles transport through quartz-Sand porous medium.** Different characterizations were carried out on the quartz-sand sample before the column experiments. The SEM analysis from quartz-sand grains depicted that the surface of grains is smooth (Fig. 3a). Furthermore, the XRD and EDX analyses from the quartz sample also revealed that the main mineral in the sample is quartz (SiO<sub>2</sub>) without any impurities (Fig. 3a). Besides that, the quartz-sand surface charge was measured as  $-36.2 \pm 0.5$  mV.

Once the columns were packed, their porosities ( $\varphi$ ) and permeability coefficients ( $k$ ) were firstly measured. The average  $\varphi$  and  $k$  of the packed columns were measured as 43% and  $2.96 \times 10^{-12}$  m<sup>2</sup> respectively. The tracer tests demonstrated that the flow path was open and the injected KNO<sub>3</sub> solution was eluted entirely after injection of 2 PVs of DIW (Fig. 4a). Thereafter, the NPs transport tests were carried out. The first transport test was carried out by Al<sub>2</sub>O<sub>3</sub>-NP suspension. Presence of Al<sub>2</sub>O<sub>3</sub>-NPs was observed in the outlet after 1.4 PVs injection. The NP concentration in the effluent moderately increased until 5.0 PVs. Then, the NP concentration ( $C/C_0$ ) values fluctuated around 0.04 until the 25<sup>th</sup> PVs. Thereafter, the NPs concentration declined to zero at the 28<sup>th</sup> PVs. After that, Al<sub>2</sub>O<sub>3</sub>-NPs were not observed in the outlet even after addition of extra 10 PVs of DIW. The result demonstrated that 47.6% of the entered Al<sub>2</sub>O<sub>3</sub>-NPs were recovered from the column. The NP breakthrough curve is demonstrated in Fig. 4a.

The surface charge of NPs is a primary factor in their transport through porous media<sup>43</sup>. The low Al<sub>2</sub>O<sub>3</sub>-NP recovery from the column is attributed to the huge difference between electric surface charges of Al<sub>2</sub>O<sub>3</sub>-NPs ( $+19.1 \pm 0.3$  mV) and quartz-sand grains ( $-36.2 \pm 0.5$  mV). According to DLVO theory (Figure S1a), the electrostatic barrier energy height between Al<sub>2</sub>O<sub>3</sub>-NPs and quartz-sand grains is negative indicating that there is an attraction force (VDW) between NPs and quartz-sand grains. As a result of this attraction force, the affinity of Al<sub>2</sub>O<sub>3</sub>-NPs to attach to the quartz-sand grains surfaces is high. Thus, the attachment process is the key retention mechanism for Al<sub>2</sub>O<sub>3</sub>-NPs in the quartz-sand porous medium. The attachment of Al<sub>2</sub>O<sub>3</sub>-NPs on the quartz-sand grains surfaces was also confirmed by FESEM and EDX analyses. Figure 5a shows that Al<sub>2</sub>O<sub>3</sub>-NPs are widely attached on the surfaces of quartz-sand grains. The values of Al<sub>2</sub>O<sub>3</sub>-NPs attachment efficiency, maximum transport distance, and deposition coefficient rate, calculated from filtration theory are shown in Table 1. Darlington *et al.*<sup>2</sup> also found that Al<sub>2</sub>O<sub>3</sub>-NPs are strongly attached to the soil and sand grains surfaces.

The second transport test using TiO<sub>2</sub>-NPs through quartz-sand porous media was carried out. The NPs appeared in the outlet after 1.2 PVs injection. The TiO<sub>2</sub>-NPs breakthrough curve is shown in Fig. 4a. The result revealed that 51.7% of the influent TiO<sub>2</sub>-NPs was recovered from the column. A low TiO<sub>2</sub> NP recovery is due to the difference in electric surface charge signs of TiO<sub>2</sub>-NPs ( $+9.1 \pm 0.3$  mV) and quartz-sand grains ( $-36.2 \pm 0.5$  mV). Dunphy Guzman *et al.*<sup>43</sup> declared that surface charge of TiO<sub>2</sub>-NPs

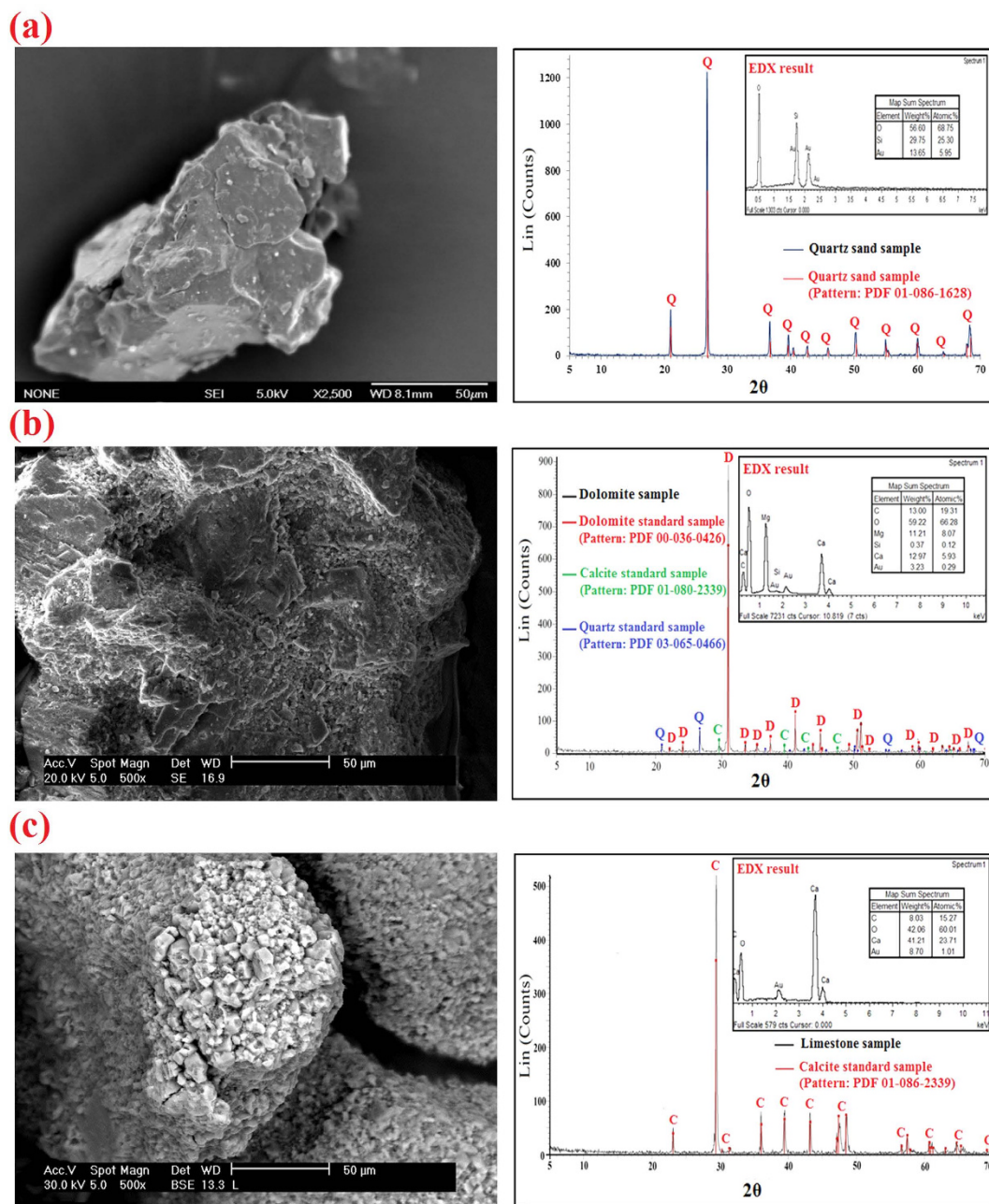


**Figure 3.** SEM, XRD, and EDX analyses results from porous media (a) quartz sand, (b) dolomite, (c) limestone.

is a primary factor in their transport through soils. Choy *et al.*<sup>44</sup> and Godinez and Darnault<sup>21</sup> observed that TiO<sub>2</sub>-NPs adsorbed highly on sand grains surfaces due to their opposite surface charge signs. Moreover, Chen *et al.*<sup>28</sup> reported a successful transport of TiO<sub>2</sub>-NPs through sand grains. They reported that TiO<sub>2</sub>-NPs and sand grains had similar surface charge signs as both were reported to be negative.

According to DLVO theory, the electrostatic barrier energy height between TiO<sub>2</sub>-NPs and quartz grains is negative which reveals attraction is the dominant force (Figure S1a). Therefore, the attachment process is the key retention mechanism for TiO<sub>2</sub>-NPs in quartz-sand porous media. The NPs attachment to the grains surfaces was also proven via FESEM and EDX analyses (Fig. 5b). The values of attachment efficiency, maximum transport distance, and deposition coefficient rate calculated by filtration theory were 0.171, 37.3 cm, and 4.72 (h<sup>-1</sup>), respectively (Table 1).

Transport of SiO<sub>2</sub>-NPs through quartz-sand porous medium was the last test. SiO<sub>2</sub>-NPs were observed in the outlet immediately after injecting the first PV (Fig. 4a). Concentration of SiO<sub>2</sub>-NPs in the effluent sharply increased to 0.148 in the 9.8<sup>th</sup> PV. Thereafter, it temperately dropped to zero at 21.8<sup>th</sup> PV. 95.6% of the entered SiO<sub>2</sub>-NPs was collected from the column. The high SiO<sub>2</sub>-NP recovery is attributed to its

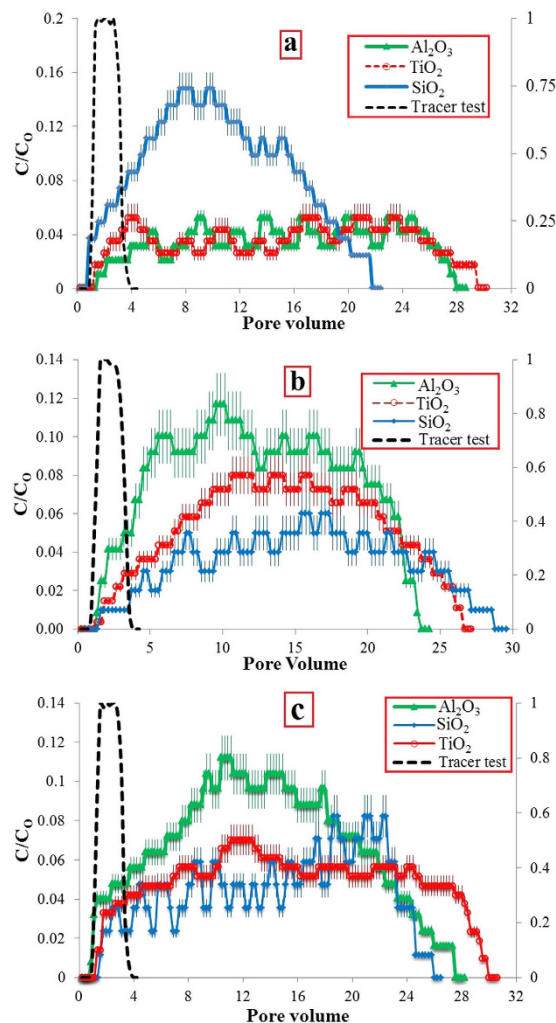


**Figure 4.** NPs breakthrough curves transported through various porous media; (a) quartz sand, (b) dolomite, (c) limestone. Breakthrough curve for the tracer test is also demonstrated; Right y-axis for tracer ( $KNO_3$ )  $C/C_0$  and left y-axis is for NPs  $C/C_0$ .

stability in DIW as well as the electric surface charge of  $SiO_2$ -NPs ( $-28.1 \pm 0.3$  mV) and quartz-sand grains ( $-36.2 \pm 0.5$  mV) which are both negative. According to DLVO theory, there is a relatively strong electrostatic barrier energy between  $SiO_2$ -NPs and quartz-sand grains which indicates a strong repulsion (EDL) force between them. As a result of this repulsion force, the affinity of  $SiO_2$ -NPs to attach to the sand grains surfaces was quite low.

**Nanoparticles transport through dolomite porous medium.** Based on SEM analysis, the surface of dolomite grains was detected to be rough and full of irregular dents and bumps (Fig. 3b). Moreover, the XRD and EDX results revealed that the sample is composed mainly of calcium magnesium carbonate,  $CaMg(CO_3)_2$ . Small amounts of quartz were also detected in this sample (Fig. 3b). Besides that, the dolomite surface charge was measured as  $+26.1 \pm 0.5$  mV.

The average  $\varphi$  and  $k$  of the packed columns were measured as 42% and  $3.19 \times 10^{-12}$  m<sup>2</sup> respectively. The tracer tests demonstrated that the flow path is open and the injected  $KNO_3$  solution was eluted entirely after injection of 2 PVs of DIW.

The first transport test was run by  $Al_2O_3$ -NP suspension. The  $Al_2O_3$ -NPs breakthrough curve is shown in Fig. 4b. The result demonstrated that 89.6% of injected  $Al_2O_3$ -NPs was recovered from the column. The high  $Al_2O_3$ -NP recovery is attributed to the electric surface charge signs of  $Al_2O_3$ -NPs ( $+19.1 \pm 0.3$  mV) and dolomite grains ( $+26.1 \pm 0.5$  mV) which are both positive. Based on DLVO theory, there is a strong electrostatic barrier energy between  $Al_2O_3$ -NPs and dolomite grains which depicts a strong repulsion force between  $Al_2O_3$ -NPs and grains (Figure S1b). As a result of this repulsion force, the affinity of  $Al_2O_3$ -NPs to attach to the dolomite grains surfaces was low. However, a small amount of  $Al_2O_3$ -NPs (10.4%) remained in the porous medium and this can be attributed to the roughness of the

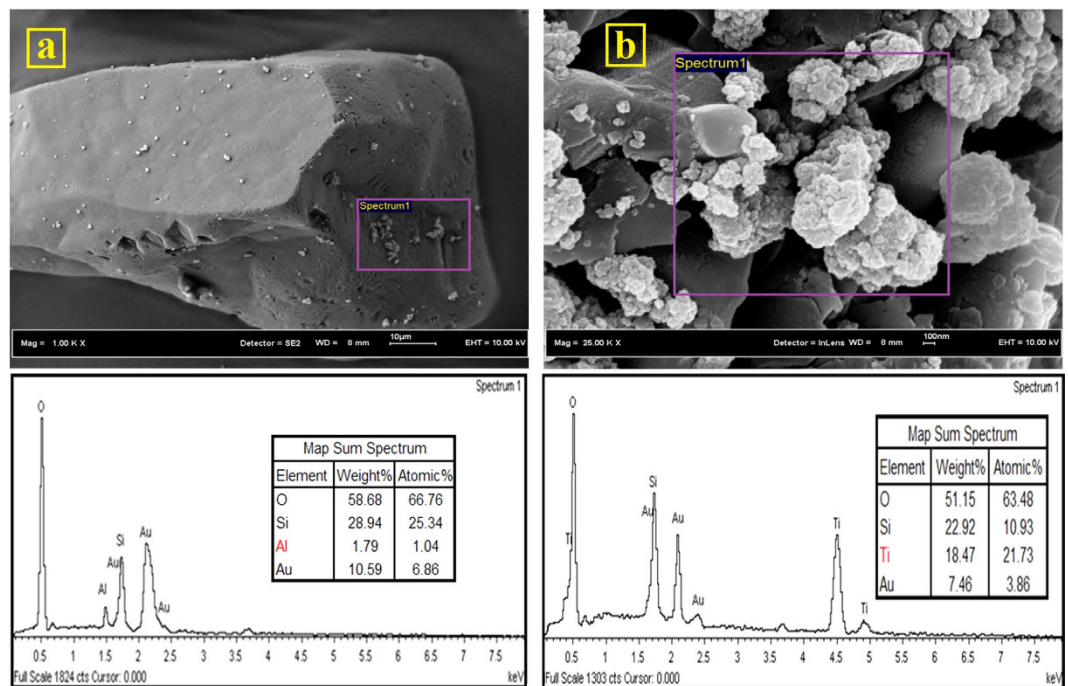


**Figure 5.** (a) FESEM-EDX analyses from quartz sand grains after the transport experiments, (a) Al<sub>2</sub>O<sub>3</sub>-NPs, (b) TiO<sub>2</sub>-NPs. (The images were taken from grains located in the entrance of columns).

surface of dolomite grains and presence of small amounts of quartz in the sample. According to filtration theory, the values of attachment efficiency, maximum transport distance, and deposition coefficient rate, for Al<sub>2</sub>O<sub>3</sub>-NP transport through dolomite porous medium, were calculated to be 0.134, 44.5 cm and 4.14 (h<sup>-1</sup>) respectively (Table 1).

The next transport experiment was performed by TiO<sub>2</sub>-NP suspension. The result depicted that 68.8% of TiO<sub>2</sub>-NPs influent was recovered from the column. The surface charges of TiO<sub>2</sub> (+9.1 ± 0.3 mV) and dolomite grains (+26.1 ± 0.5 mV) are both positive. According to DLVO, the interaction energy barrier is positive which depicts that a repulsion force exists between TiO<sub>2</sub>-NPs and dolomite grains. However, one third of the entered TiO<sub>2</sub>-NPs remained in the porous medium. To know why the NPs retained in the porous medium, the results from this test should be compared with Al<sub>2</sub>O<sub>3</sub>-NPs transport test. According to DLVO, the maximum interaction energy ( $k_B T$ ) height value for TiO<sub>2</sub> NP-NP is one sixth of the interaction energy height for Al<sub>2</sub>O<sub>3</sub> NP-NP (Table 1) which shows stronger repulsion force among Al<sub>2</sub>O<sub>3</sub>-NPs. Thus, the stability of Al<sub>2</sub>O<sub>3</sub>-NPs in DIW against deposition is higher than TiO<sub>2</sub>-NPs. Yu *et al.*<sup>14</sup> and Bayat *et al.*<sup>29,30</sup> stated that mobility of NPs through a porous medium is a function of their stabilities where lower stabilities lead to mobility reduction. In addition, the interaction energy height between Al<sub>2</sub>O<sub>3</sub>-NPs and dolomite grains is 4.4 folds higher than TiO<sub>2</sub>-NPs and dolomite grains. This depicts that the repulsion force between Al<sub>2</sub>O<sub>3</sub>-NPs and dolomite grains is much greater than TiO<sub>2</sub>-NPs and dolomite grains (Table 1). In addition, according to filtration theory, the values of attachment efficiency and deposition rate coefficient for TiO<sub>2</sub>-NPs in dolomite porous media are also 1.25 times higher than Al<sub>2</sub>O<sub>3</sub>-NPs as shown in Table 1. The value of attachment efficiency has direct relationship with the amount of NP recovery where higher values of attachment efficiency lead to lower amounts of NPs recovery from the column<sup>21,30,31,45</sup>. These are the reasons why Al<sub>2</sub>O<sub>3</sub>-NPs recovery value in dolomite porous media is higher in comparison to TiO<sub>2</sub>-NPs. Consequently, deposition process is the key retention mechanism for TiO<sub>2</sub>-NPs in the dolomite porous medium. Results of the FESEM and EDX analyses show that the deposited TiO<sub>2</sub>-NPs were also observed on the grains surfaces located in the middle of column (Fig. 6a).

SiO<sub>2</sub>-NPs transport was the last test through dolomite porous medium. The outcome revealed that only 48.6% of the entered SiO<sub>2</sub>-NPs in the column was recovered. Difference in the electric surface charge signs of SiO<sub>2</sub>-NPs (-28.1 ± 0.3 mV) and dolomite grains (+26.1 ± 0.5 mV) caused the NPs to attach strongly to the dolomite grains surfaces. The result of DLVO theory demonstrates that there is an attraction force between SiO<sub>2</sub>-NPs and sand grains (Figure S1b). Consequently, FESEM and EDX measurements were carried out to observe the attached NPs. As shown in Fig. 6b, SiO<sub>2</sub>-NPs were widely attached to the dolomite grains surfaces. As mentioned in Nanoparticles characterizations section, the NPs in DIW aggregated and made bigger clusters. The bigger NPs clusters during transport through porous media can trap behind the tiny pore-throats which this phenomenon is called straining. The trapped clusters may then make networks up to micron size especially when the NPs and porous media

Porous media	NP suspension	DLVO Theory				Filtration Theory				$R_{NP}$ (%)
		NPs $\zeta$ -potential (mV)	Maximum value of NP-NP interaction energy height	Porous media $\zeta$ -potential (mV)	Maximum value of NP- medium interaction energy height	Single-collector contact efficiency, $\eta_0 = \eta_D + \eta_I + \eta_G$	Attachment efficiency, $\alpha$	Maximum transport distance, $L_{max}$ (cm)	Deposition rate coefficient, $k_d$ ( $h^{-1}$ )	
Quartz sand	Al <sub>2</sub> O <sub>3</sub>	+19.1 ± 0.3	+30.2	-36.2 ± 0.5	negative	1.34E-02	0.182	33.0	5.46	47.6
	TiO <sub>2</sub>	+9.1 ± 0.3	+5.2		negative	1.30E-02	0.169	37.3	4.72	51.7
	SiO <sub>2</sub>	-28.1 ± 0.3	+57.1		+194.5	1.19E-02	0.132	50.4	3.66	95.6
Dolomite	Al <sub>2</sub> O <sub>3</sub>	+19.1 ± 0.3	+30.2	+26.1 ± 0.5	+82.1	1.33E-02	0.134	44.5	4.14	89.6
	TiO <sub>2</sub>	+9.1 ± 0.3	+5.2		+18.6	1.25E-02	0.168	37.3	5.06	68.8
	SiO <sub>2</sub>	-28.1 ± 0.3	+57.1		negative	1.23E-02	0.203	33.0	5.33	48.6
Limestone	Al <sub>2</sub> O <sub>3</sub>	+19.1 ± 0.3	+30.2	+33.1 ± 0.5	+88.3	1.35E-02	0.127	47.2	3.81	91.8
	TiO <sub>2</sub>	+9.1 ± 0.3	+5.2		+19.1	1.26E-02	0.143	44.2	4.18	72.2
	SiO <sub>2</sub>	-28.1 ± 0.3	+57.1		negative	1.24E-02	0.168	40.3	4.27	56.6

**Table 1.** Electrokinetic properties of NPs and porous media, energy barrier heights as calculated by DLVO theory for NP-NP and NP-porous medium interactions as well as experimental parameters from NPs transport tests calculated by filtration theory.

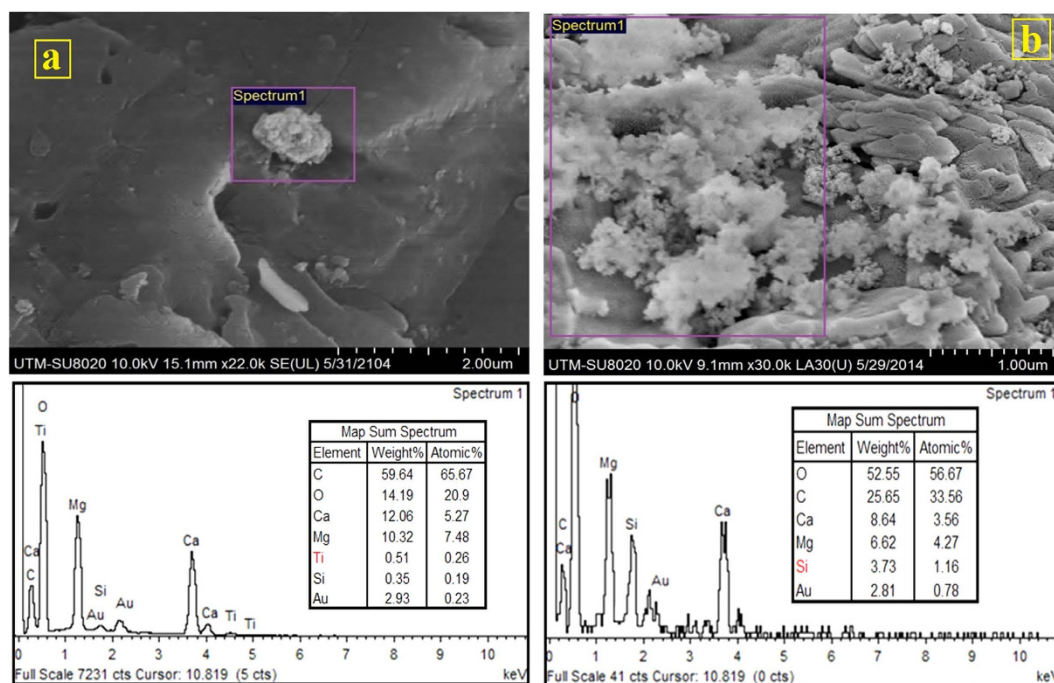


**Figure 6.** (a) FESEM-EDX analyses from dolomite grains after the transport experiments, (a) TiO<sub>2</sub>-NPs, (b) SiO<sub>2</sub>-NPs. (Right image was taken from a grain located in the top of column and left image was taken from a grain located in the entrance of column).

grains surface charges are in contrast. Therefore, the NPs aggregates observed in the some FESEM images. Furthermore, based on filtration theory, the values of attachment efficiency, maximum transport distance, and deposition rate were calculated to be 0.203, 33 cm and  $5.33 h^{-1}$  respectively (Table 1).

**Nanoparticles transport through limestone porous medium.** From the SEM analysis, the surface of limestone grains was detected to be rough and full of irregular dents and bumps which are similar to dolomite grains (Fig. 3c). Furthermore, the XRD and EDX results revealed that the sample is composed purely of calcite, CaCO<sub>3</sub>. The limestone surface charge was also measured as  $+33.1 \pm 0.5$  mV.



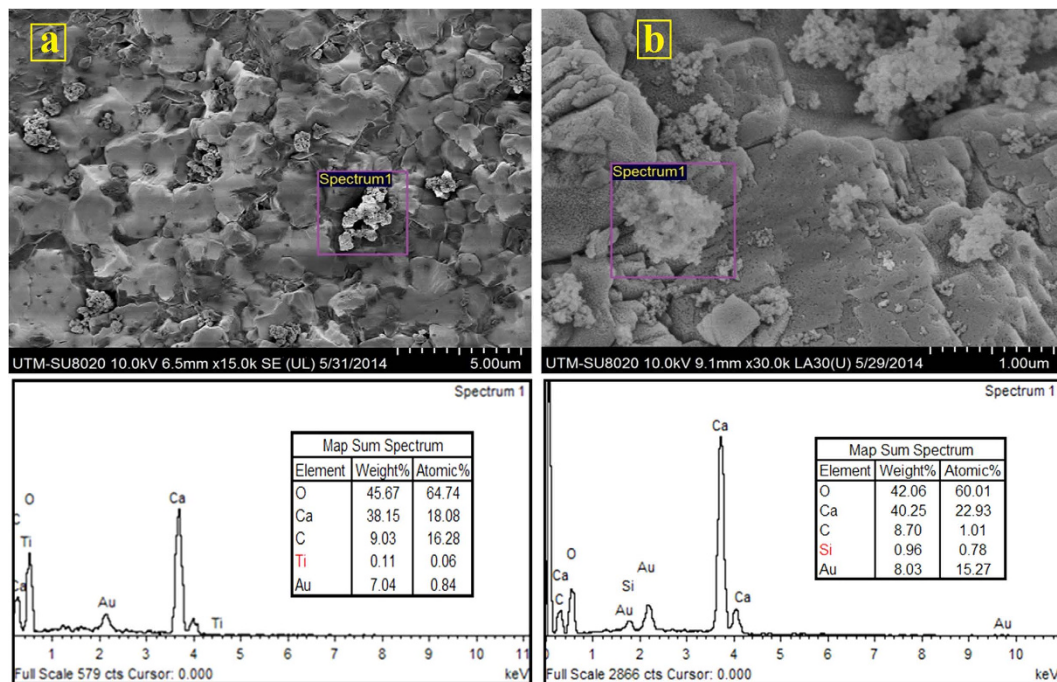


**Figure 7.** (a) FESEM-EDX analyses from limestone grains after the transport experiments, (a) TiO<sub>2</sub>-NPs, (b) SiO<sub>2</sub>-NPs. (Right image was taken from a grain located in the top of column and left image was taken from a grain located in the entrance of column).

The average  $\varphi$  and  $k$  of the packed columns were measured as 44% and  $3.05 \times 10^{-12} \text{ m}^2$  respectively. The tracer tests results depicted that the flow path is open (Fig. 4c). The breakthrough curves for Al<sub>2</sub>O<sub>3</sub>, TiO<sub>2</sub>, and SiO<sub>2</sub> NPs transport tests through limestone porous media are also shown in Fig. 4c. The results demonstrated that 91.8% of injected Al<sub>2</sub>O<sub>3</sub>-NPs, 72.2% of TiO<sub>2</sub>-NPs, and 56.6% of SiO<sub>2</sub>-NPs were recovered from the columns. The interaction energy curves between NPs and limestone grains were drawn based on DLVO theory. The maximum and minimum interaction energy heights belong to Al<sub>2</sub>O<sub>3</sub> and SiO<sub>2</sub> NPs (Table 1). The reasons for the high and/or low NPs recovery have been explained in the previous sections. Deposition and attachment respectively were detected as the key retention mechanisms for TiO<sub>2</sub> and SiO<sub>2</sub> NPs on limestone grains. Accordingly, the FESEM and EDX measurements proved the presence of TiO<sub>2</sub> and SiO<sub>2</sub> NPs on the limestone grains surfaces (Fig. 7). In addition, based on filtration theory, the maximum values for the both attachment efficiency and deposition rate coefficient parameters in the limestone porous media were obtained for SiO<sub>2</sub>-NPs while the minimum values of the mentioned parameters were achieved for Al<sub>2</sub>O<sub>3</sub>-NPs (Table 1).

The outcomes from this study are of interest to those in the environmental and petroleum engineering fields. Generally, NPs transport and retention through various porous media was found to be strongly dependent on NP stability in suspension against deposition, NP surface charge as well as porous media surface charge and roughness. The more stable NPs which have the same surface charge sign as porous media can easily transport while contrast in surface charge sign between NPs and porous media leads to NPs to attach to the porous media grains surfaces. Consequently, the quantities of Al<sub>2</sub>O<sub>3</sub>, TiO<sub>2</sub>, and SiO<sub>2</sub> NPs recoveries from quartz-sand porous media were totally different from the carbonates (limestone and dolomite) porous media. For Al<sub>2</sub>O<sub>3</sub> and TiO<sub>2</sub> NPs, attachment process is the key retention mechanism through the quartz-sand porous medium. Moreover, it was observed that TiO<sub>2</sub>-NPs recoveries through the carbonates porous media were lower than Al<sub>2</sub>O<sub>3</sub>-NPs recoveries. The reason is related to the lower stability of TiO<sub>2</sub>-NPs in DIW as compared to Al<sub>2</sub>O<sub>3</sub>-NPs. Deposition and attachment processes have been identified as key retention mechanisms for TiO<sub>2</sub>-NPs and SiO<sub>2</sub>-NPs in the carbonates porous media.

## Methods

**NPs suspension preparation and characterization.** Three commercial nanopowders, SiO<sub>2</sub> (20 nm, non-porous), Al<sub>2</sub>O<sub>3</sub> (40 nm, alpha-Al<sub>2</sub>O<sub>3</sub>), and TiO<sub>2</sub> (10–30 nm, anatase-TiO<sub>2</sub>) received from SkySpring Nanomaterials, Inc., (Houston, TX), were utilized in this study. X-ray diffraction (XRD, model D5000, SIMENS) and transmission electron microscopy (TEM, model JEM-2100/HR, JEOL, Acc.200.00 kV) analyses were carried out to recheck the NPs crystalline compositions, sizes, and morphologies. Al<sub>2</sub>O<sub>3</sub>, TiO<sub>2</sub>, and SiO<sub>2</sub> NPs suspensions were prepared by adding 50 mg of each nano powder to 1 liter of de-ionized water (DIW) at pH  $6.4 \pm 0.1$ . The reason for selecting DIW as the dispersion medium was to avoid the effects of solution chemistry (i.e. ionic strength and pH) on the NPs stability and transport. The

suspensions were agitated for 1 hr using an orbital shaker at 220 rpm and ultrasonicated by an ultrasonic bath for a period of 1 hr to obtain homogenous suspensions prior to each test. The NPs suspensions preparation was carried out 15 min prior to the tests.

For the experiments, the average  $\zeta$ -potential values of the NPs in DIW were measured via a zeta potential analyzer instrument (ZEECOM Microtec Co., Ltd). The NPs suspensions were prepared, sonicated for 1 hr and shaken prior used for the  $\zeta$ -potential measurements. The  $\zeta$ -potential values were obtained by averaging three  $\zeta$ -potential measurements for all NPs suspensions. Furthermore, the average NP aggregates radiuses in DIW were measured using a DynaPro Titan Dynamic Light Scattering (DLS) probe from Wyatt Technology Corporation. Then, the NPs suspensions were prepared for  $\zeta$ -potential measurements. DLS scattering analyses were performed thrice (20 DLS reading per each run) for each NP suspension. The mean value of the measurements was applied to determine the radius of NPs aggregates. All these characterization techniques were conducted at room temperature (26°C).

**Sedimentation tests.** The stability of  $\text{Al}_2\text{O}_3$ ,  $\text{TiO}_2$ , and  $\text{SiO}_2$  NPs in DIW against deposition was determined through sedimentation experiments. The sedimentation tests were carried out in the static condition where there was no movement in the suspensions. The amount of NPs deposition was recorded for each 5 min intervals over a 180 min time span with the use of time-resolved optical absorbance. The absorbance of the samples was measured using an ultraviolet visible (UV-VIS) spectrophotometer (model 105, BUCK SCIENTIFIC, Inc.) over the wavelength range of 200–800 nm. Calibration was based on the maximum absorbance wavelength of 400 nm. These experiments were repeated twice and the presented data is the average of the obtained records.

**Porous media preparation and characterization.** Natural limestone (from a surface outcrop in Ipoh, Malaysia), dolomite (from Ward's Natural Science Establishment, Inc., Minnesota, NY, US), and quartz-sand (from Desaru seaside, Johor Malaysia) were utilized as the porous media used in this study. The samples of limestone and dolomite were received as large blocks. The blocks were broken off into the smaller pieces and then crushed to fine grains using a crusher machine (PULVERIZER Type from BICO, Inc.). The limestone, dolomite, and quartz-sand grains were sifted through 125 and 175  $\mu\text{m}$  stainless steel sieves (USA Standard Testing Sieves, ATM Corp., New Berlin, WI) to achieve an average collector diameter ( $d_c$ ) of 150  $\mu\text{m}$ . The limestone and dolomite fractions were pre-treated using a sequential water rinse, ultrasonication, and oven-drying procedure at 110°C for 12 hours to eliminate impurities. The quartz-sand grains were also cleaned from impurities by soaking them in 12N HCL acid (Fisher Scientific) for 24 hours, washing in de-ionized water (DIW), and baking at 250°C for 12 hours<sup>28</sup>. The densities of limestone, dolomite, and quartz-sand samples after pre-treatment were measured according to the ASTM standard D 854–14 method<sup>46</sup> as 2.67, 2.83, and 2.52  $\text{g}/\text{cm}^3$  respectively. Following that, scanning electron microscope (SEM, Philips XL40) and field emission scanning electron microscopy (FESEM, HITACHI, SU8020) images were prepared from the limestone, dolomite, and quartz-sand grains to determine the exact morphology of the grains before and after performing the transport experiments. Besides that, energy dispersive X-ray (EDX) and XRD analyses were also carried out to determine the limestone, dolomite and quartz-sand compositions before and after the transport tests. The  $\zeta$ -potential values of the cleaned samples were also measured using the method detailed by Tufenkj and Elimelech<sup>45</sup>.

**Column transport tests.** For each experimental trial, the cleaned limestone, dolomite, and quartz-sand grains averaging 30.8, 32.8, and 29.3 gr respectively were placed into stainless steel tube with an inner diameter of 0.9 cm and a length of 33 cm. A 50 micron filter cloth was placed at both ends of the tube to prevent grain migration during displacement tests. The column was then wet packed uniformly with cleaned grains using the method explained by Chen *et al.*<sup>28</sup>. Once the column was packed, it was saturated in a vertical upward direction using a syringe pump (Model PSK-01; NIKKISO Co., Ltd) at a constant Darcy velocity of  $4.66 \times 10^{-3} \text{ cm}/\text{sec}$  (flow rate of 1  $\text{cm}^3/\text{min}$ ) with approximately 10 pore volumes (PVs) of DIW to ensure a homogenous saturation of the pack. It should be noted that the flow direction was selected to be vertically upward to equilibrate the influent solution and enhance packing homogeneity<sup>21</sup>. Once the column was homogeneously packed and saturated, a pulse of each NP suspension (50 mg/L) with Darcy velocity of  $4.66 \times 10^{-3} \text{ cm}/\text{sec}$  was injected into the column for 2 PVs. Thereafter, DIW was injected into the column until no NP was observed in the outlet as a means to check for mobilization of trapped NPs in the porous medium. At the same time, the effluents were collected using a fraction collector (CF-2, Spectrum Chromatography, Houston, TX, USA) in 2 ml sample sizes. On average, 170 effluent samples were collected after each conducted experiment. The NPs concentration in the collected samples was measured using an UV-VIS spectrophotometer (Model 105, BUCK SCIENTIFIC, Inc.) over the wavelength range of 200–800 nm. Calibration was based on a maximum absorbance wavelength of 400 nm. Finally, the concentration of NPs dispersions entering the porous medium  $C_0$ , and in the outlet  $C$  were applied to generate breakthrough curves of  $C/C_0$  as function of PVs passing through the porous media. All transport experiments were duplicated and data expressed is the standard error of mean.

Prior to transport tests, a tracer test was also carried out using a 50 mM potassium nitrate ( $\text{KNO}_3$ ) solution to determine the water flow characteristics and column performance. The selection of  $\text{KNO}_3$  is

related to its stability and non-reactive species<sup>28</sup>. 2PVs of KNO<sub>3</sub> were injected into the porous media. Consequently, DIW was injected and the outlets were collected in 2 ml samples. The concentration of KNO<sub>3</sub> in the outlet was measured using a conductivity probe (Thermo Scientific Orion 3-Star). Finally, the concentration of KNO<sub>3</sub> entering the column C<sub>0</sub>, and in the outlet C was applied to generate breakthrough curves of C/C<sub>0</sub> as function of PVs passing through the column.

**Colloids transport theories.** The transport tests results were cross checked by classical DLVO and filtration theories. These theories were applied to qualitatively and quantitatively assess and explain the NPs transport and retention through porous media<sup>29,30</sup>. The details of these theories are illustrated in the supplementary file.

## References

- Jiang, X., Tong, M., Lu, R. & Kim, H. Transport and deposition of ZnO nanoparticles in saturated porous media. *Colloids and Surfaces A: Physicochemical and Engineering Aspects* **401**, 29–37 (2012).
- Darlington, T. K., Neigh, A. M., Spencer, M. T., Nguyen, O. T. & Oldenburg, S. J. Nanoparticle characteristics affecting environmental fate and transport through soil. *Environ. Toxicol. Chem./SETAC* **28**, 1191–1199 (2009).
- Nel, A., Xia, T., Mädler, L. & Li, N. Toxic Potential of Materials at the Nanolevel. *Science* **311**, 622–627 (2006).
- Scown, T. M., van Aerle, R. & Tyler, C. R. Review: Do engineered nanoparticles pose a significant threat to the aquatic environment? *Critical Reviews in Toxicology* **40**, 653–670 (2010).
- Bour, A., Mouchet, F., Silvestre, J., Gauthier, L. & Pinelli, E. Environmentally relevant approaches to assess nanoparticles ecotoxicity: A review. *J Hazardous Materials* **283**, 764–777 (2015).
- Fang, Q. *et al.* Effect of titanium dioxide nanoparticles on the bioavailability, metabolism, and toxicity of pentachlorophenol in zebrafish larvae. *J Hazardous Materials* **283**, 897–904 (2015).
- Krewski, D. *et al.* Rondeau, Human Health Risk Assessment for Aluminum, Aluminum Oxide and Aluminum Hydroxide. *J Toxicol Environ Health B Crit Rev.* **10**, 1–269 (2007).
- Jaisi, D. P., Saleh, N. B., Blake, R. E. & Elimelech, M. Transport of Single-Walled Carbon Nanotubes in Porous Media: Filtration Mechanisms and Reversibility. *Environ. Sci. Technol.* **42**, 8317–8323 (2008).
- Chowdhury, I., Hong, Y., Honda, R. J. & Walker, S. L. Mechanisms of TiO<sub>2</sub> nanoparticle transport in porous media: Role of solution chemistry, nanoparticle concentration, and flowrate. *J Colloid and Interface Science* **360**, 548–555 (2011).
- Handy, R. D. & Shaw, B. J. Toxic effects of nanoparticles and nanomaterials: Implications for public health, risk assessment and the public perception of nanotechnology. *Health, Risk & Society* **9**, 125–144 (2007).
- Esfandiyari Bayat, A., Junin, R., Samsuri, A., Piroozian, A. & Hokmabadi, M. Impact of Metal Oxide Nanoparticles on Enhanced Oil Recovery from Limestone Media at Several Temperatures. *Energy Fuels* **28**, 6255–6266 (2014).
- Ehtesabi, H., Ahadian, M. M., Taghikhani, V. & Ghazanfari, M. H. Enhanced Heavy Oil Recovery in Sandstone Cores Using TiO<sub>2</sub> Nanofluids. *Energy Fuels* **28**, 423–430 (2014).
- Hendraningrat, L., Torsæter, O. Metal oxide-based nanoparticles: revealing their potential to enhance oil recovery in different wettability systems. *Appl. Nanosci.* **5**, 181–199 (2015).
- Yu, J., An, C., Mo, D., Liu, N. & Lee, R. L. Study of Adsorption and Transportation Behavior of Nanoparticles in Three Different Porous Media. *SPE Improved Oil Recovery Symposium*, Tulsa, Oklahoma, USA, April 14–18, (2012), doi: 10.2118/153337-MS.
- Lecoanet, H. F., Bottero, J. Y. & Wiesner, M. R. Laboratory Assessment of the Mobility of Nanomaterials in Porous Media. *Environ. Sci. Technol.* **38**, 5164–5169 (2004).
- Auffan, M. *et al.* Towards a definition of inorganic nanoparticles from an environmental, health and safety perspective, *Nat Nano* **4**, 634–641 (2009).
- Jiang, J., Oberdörster, G. & Biswas, P. Characterization of size, surface charge, and agglomeration state of nanoparticle dispersions for toxicological studies. *J Nanopart Res.* **11**, 77–89 (2009).
- Wang, C., Wei, J., Xia, B., Chen, X. & He, B. Effect of nano-silica on the mechanical, thermal, and crystalline properties of poly(vinyl alcohol)/nano-silica films. *J Applied Polymer Sci.* **128**, 1652–1658 (2013).
- Alaskar, M. *et al.* Horne, Nanoparticle and Microparticle Flow in Porous and Fractured Media: An Experimental Study. *SPE Annual Technical Conference and Exhibition* Denver, Colorado, USA, October 30 -November 2 (2011), doi: 10.2118/146752-MS.
- Phenrat, T. *et al.* Stabilization of aqueous nanoscale zerovalent iron dispersions by anionic polyelectrolytes: adsorbed anionic polyelectrolyte layer properties and their effect on aggregation and sedimentation. *J Nanopart Res.* **10**, 795–814 (2008).
- Godínez, I. G. & Darnault, C. J. G. Aggregation and transport of nano-TiO<sub>2</sub> in saturated porous media: Effects of pH, surfactants and flow velocity. *Water Research* **45**, 839–851 (2011).
- Aiken, G. R., Hsu-Kim, H. & Ryan, J. N. Influence of Dissolved Organic Matter on the Environmental Fate of Metals, Nanoparticles, and Colloids. *Environ. Sci. Technol.* **45**, 3196–3201 (2011).
- Saleh, N. *et al.* Ionic Strength and Composition Affect the Mobility of Surface-Modified Fe0 Nanoparticles in Water-Saturated Sand Columns. *Environ. Sci. Technol.* **42**, 3349–3355 (2008).
- Thio, B. J. R., Zhou, D. & Keller, A. A. Influence of natural organic matter on the aggregation and deposition of titanium dioxide nanoparticles. *Journal of Hazardous Materials* **189**, 556–563 (2011).
- Kim, C. & Lee, S. Effect of seepage velocity on the attachment efficiency of TiO<sub>2</sub> nanoparticles in porous media. *Journal of Hazardous Materials* **279**, 163–168 (2014).
- French, R. A. *et al.* Influence of Ionic Strength, pH, and Cation Valence on Aggregation Kinetics of Titanium Dioxide Nanoparticles. *Environ. Sci. Technol.* **43**, 1354–1359 (2009).
- Ben-Moshe, T., Dror, I. & Berkowitz, B. Transport of metal oxide nanoparticles in saturated porous media. *Chemosphere* **81**, 387–393 (2010).
- Chen, G., Liu, X. & Su, C. Transport and Retention of TiO<sub>2</sub> Rutile Nanoparticles in Saturated Porous Media under Low-Ionic-Strength Conditions: Measurements and Mechanisms. *Langmuir* **27**, 5393–5402 (2011).
- Esfandiyari Bayat, A., Junin, R., Ghadikolaei, F. D. & Piroozian, A. Transport and aggregation of Al<sub>2</sub>O<sub>3</sub> nanoparticles through saturated limestone under high ionic strength conditions: measurements and mechanisms. *J Nanopart Res.* **16**, 1–12 (2014).
- Esfandiyari Bayat, A., Radzuan, J., Derahman, M. N. & Samad, A. TiO<sub>2</sub> nanoparticle transport and retention through saturated limestone porous media under various ionic strength conditions. *Chemosphere* **134**, 7–15 (2015).
- Fang, J., Shan, X. Q., Wen, B., Lin, J. M. & Owens, G. Stability of titania nanoparticles in soil suspensions and transport in saturated homogeneous soil columns. *Environmental Pollution* **157**, 1101–1109 (2009).
- Cai, L., Tong, M., Wang, X. & Kim, H. Influence of Clay Particles on the Transport and Retention of Titanium Dioxide Nanoparticles in Quartz Sand. *Environ. Sci. Technol.* **48**, 7323–7332 (2014).

33. Esfandyari Bayat, A., Junin, R., Mohsin, R., Hokmabadi, M. & Shamshirband, Sh. Influence of Clay Particles on Al<sub>2</sub>O<sub>3</sub> and TiO<sub>2</sub> Nanoparticles Transport and Retention through Limestone Porous Media: Measurements and Mechanisms. *J Nanopart Res.* **17**(5), 1–14 (2015).
34. Freas, R. C., Hayden, J. S. & Pryor Jr, C. A. Limestone and dolomite. In: Kogel, J. E., Trivedi, N. C., Barker, J. M., Krukowski, S. T. (Eds.), *Industrial Minerals and Rocks: Commodities, Markets and Uses* seventh Ed. Society for Mining, Metallurgy, and Exploration, Littleton, 2006, 581–597 (2006).
35. Petosa, A. R., Brennan, S. J., Rajput, F. & Tufenkji, N. Transport of two metal oxide nanoparticles in saturated granular porous media: Role of water chemistry and particle coating. *Water Research* **46**, 1273–1285 (2012).
36. Raiswell, R. *et al.* Contributions from glacially derived sediment to the global iron (oxyhydr)oxide cycle: Implications for iron delivery to the oceans. *Geochimica et Cosmochimica Acta* **70**, 2765–2780 (2006).
37. Yu, H. *et al.* Flow enhancement of water-based nanoparticle dispersion through microscale sedimentary rocks. *Sci. Rep.* **5**, 8702, doi: 10.1038/srep08702 (2015).
38. Salehi, M., Johnson, S. J. & Liang, J. T. Mechanistic Study of Wettability Alteration Using Surfactants with Applications in Naturally Fractured Reservoirs. *Langmuir* **24**, 14099–14107 (2008).
39. Karimi, A. *et al.* Wettability Alteration in Carbonates using Zirconium Oxide Nanofluids: EOR Implications. *Energy Fuels* **26**, 1028–1036 (2012).
40. Cullity, B. D., and Stock, S. R. *Elements of X-Ray Diffraction* Third ed., Prentice Hall, New Jersey, 2001.
41. Hotze, E. M., Phenrat, T. & Lowry, G. V. Nanoparticle Aggregation: Challenges to Understanding Transport and Reactivity in the Environment. *J of Environ. Qual.* **39**, 1909–1924 (2010).
42. Bian, S. W., Mudunkotuwa, I. A., Rupasinghe, T. & Grassian, V. H. Aggregation and Dissolution of 4 nm ZnO Nanoparticles in Aqueous Environments: Influence of pH, Ionic Strength, Size, and Adsorption of Humic Acid. *Langmuir* **27**, 6059–6068 (2011).
43. Dunphy Guzman, K. A., Finnegan, M. P. & Banfield, J. F. Influence of Surface Potential on Aggregation and Transport of Titania Nanoparticles. *Environ. Sci. Technol.* **40**, 7688–7693 (2006).
44. Choy, C. C., Wazne, M. & Meng, X. Application of an empirical transport model to simulate retention of nanocrystalline titanium dioxide in sand columns. *Chemosphere* **71**, 1794–1801 (2008).
45. Tufenkji, N. & Elimelech, M. Deviation from the Classical Colloid Filtration Theory in the Presence of Repulsive DLVO Interactions. *Langmuir* **20**, 10818–10828 (2004).
46. ASTM D854-14, Standard Test Methods for Specific Gravity of Soil Solids by Water Pycnometer, ASTM International, West Conshohocken, PA, doi: 10.1520/D0854-14 (2014).

## Acknowledgements

The authors are grateful to Department of Petroleum Engineering at Universiti Teknologi Malaysia for providing adequate facilities to conduct this research and also to the Research Management Center (RMC) of Universiti Teknologi Malaysia for financial support of this research through the Post-Doctoral Fellowship Grant with Vote No. Q.J130000.21A2.02E38. We would also to acknowledge the Ministry of Higher Education of Malaysia and the University of Malaya, Kuala Lumpur, Malaysia for additional financial support under HIRG: UM.C/HIR/MOHE/ENG/06 (D000006-16001).

## Author Contributions

A.E.B. and R.J. designed, performed, and directed the study. SH.SH. and W.T.Ch were consultant and financial supporter of this study. The manuscript was written by A.E.B. and all authors reviewed and confirmed it.

## Additional Information

**Supplementary information** accompanies this paper at <http://www.nature.com/srep>

**Competing financial interests:** The authors declare no competing financial interests.

**How to cite this article:** Esfandyari Bayat, A. *et al.* Transport and retention of engineered Al<sub>2</sub>O<sub>3</sub>, TiO<sub>2</sub>, and SiO<sub>2</sub> nanoparticles through various sedimentary rocks. *Sci. Rep.* **5**, 14264; doi: 10.1038/srep14264 (2015).



This work is licensed under a Creative Commons Attribution 4.0 International License. The images or other third party material in this article are included in the article's Creative Commons license, unless indicated otherwise in the credit line; if the material is not included under the Creative Commons license, users will need to obtain permission from the license holder to reproduce the material. To view a copy of this license, visit <http://creativecommons.org/licenses/by/4.0/>